# Simulation of the observation pipeline of the NIKA camera *(Research Note)*

R. Adam[1], N. Ponthieu[2], J. F. Macías-Pérez[1], F. X. Désert[2], A. Catalano[1], A. Benoit[3], M. Calvo[3], A. Monfardini[3]

[1] Laboratoire de Physique Subatomique et de Cosmologie, Université Joseph Fourier Grenoble 1, CNRS/IN2P3, Institut Polytechnique de Grenoble, 53, rue des Martyrs, Grenoble, France
[2] IPAG, Observatoire de Grenoble, BP 53, 38041 Grenoble, France
[3] Institut Néel, CNRS & Université Joseph Fourier, BP 166, 38042 Grenoble, France

October 2012

**ABSTRACT**

*Aims.* Test the observation pipeline with the NIKA camera.
*Methods.* We report here the method used to perform simulations of the full observation pipeline of the NIKA camera. This includes the simulation of four main steps. 1- The realistic serpentine like scan used to image astrophysical sources at the IRAM 30m telescope. 2- The simulation of the atmospheric noise. 3- The physical modeling of the detectors. 4- The reconstruction of the absorbed optical power. This pipeline allows us to construct the Time Ordered Information (TOI) for each detector.
*Results.* The simulation of the NIKA camera should be realistic enough to be used for estimating the expected outcomes of the observation of astrophysical sources. It will be used in the case of the observation of well chosen galaxy clusters, via their imprints in the Cosmic Microwave Background (CMB) due to the thermal Sunyaev-Zel'dovich effect, in order to test decorrelation techniques and to estimate the expected observed maps.

**Key words.** Kinetic Inductance Detectors – The New IRAM KIDs Array – Simulation

## 1. Introduction

The New IRAM KIDs Array (NIKA) is a $\sim$ 12 arcsec resolution instrument in development for millimeter wave observation. NIKA consists of a dual-band array of Kinetic Inductance Detectors (KIDs) at 140 GHz and 220 GHz[1]. A prototype of the camera has already been successfully tested at the Institut de Radio Astronomie Millimétrique (IRAM) 30-meters telescope at Pico Veleta (Granada, Spain), during four campaigns in October 2009 (Monfardini et al. (2010)), October 2010 (Monfardini et al. (2011)), November 2011 and June 2012. They allowed to demonstrate performances comparable to the best bolometers arrays developed to date for these wavelengths, such as GISMO (Staguhn et al. (2006)). The final instrument should be operational in 2014.

Unlike traditional instrument which use bolometers as their detectors, NIKA uses KIDs. KIDs are superconducting resonators for which the resonance frequency changes as a function of the absorbed optical power (see for example Swenson et al. (2010)). They can be modeled by a complex transfer function with real part $I$ (In-phase) and imaginary part $Q$ (Quadrature) (Grabovskij et al. (2008)), measured as a function of time. This quantities can then be use to reconstruct the shift of the resonance frequency and therefore estimate absorbed optical power (Calvo et al. (2012)).

This note presents the construction of a simulation of the NIKA camera, including the modeling of the resonances. It is divided into three main section. In the first one, we describe the operating principle of the KIDs and the way they have been modeled. The second section presents the construction of the Time Ordered Information (TOI) $I(t)$ and $Q(t)$ obtained with NIKA for a run of observation at the IRAM 30-meters telescope at Pico Veleta. It includes the sources of noise such as the atmosphere, the electronic noise and the intrinsic noise of the detectors. Finally, we expose the way the resonance frequency is reconstructed and we test this method in extreme cases.

[1] Dual-polarization LEKID (Lumped Element KID, (Doyle et al. (2008))) pixels realized on a few hundreds $\mu$m high resistivity silicon substrate. The pitch between pixels is 2.3 mm at 140 GHz, corresponding to an effective focal plane sampling of 0.75 F$\lambda$ and 1.25 F$\lambda$ at 220 GHz. The detectors are cooled down to about 100 mK with a $^4He-^3He$ dilution cryostat.

## 2. Modeling of the KIDs

### 2.1. Modeling KIDs

KIDs are high quality superconducting resonators made of an inductive line coupled to a capacity $C$ (Calvo et al. (2010)). The inductance is itself due to the sum of the geometric inductance $L_g$ and the kinetic inductance $L_k$. The resonance frequency of KIDs is given by

$$f_0 = \frac{1}{2\pi\sqrt{C\left(L_k + L_g\right)}} \tag{1}$$

Absorbed photons of high enough energy can break Cooper pairs and induce a shift in the resonance frequency due to the change of $L_k$, which is sensitive to the variation density of superconducting carriers. The frequency shift can be expressed as $\delta f_0 = -\frac{Cf_0^3}{2}\delta L_k$. For thin films, the incoming optical power $P_{opt}$ is directly proportional to the change of kinetic inductance Swenson et al. (2010). Therefore, the shift of the resonance frequency appears to be the right quantity to probe the optical power, we can assume $\delta f_0 \propto P_{opt}$.

KIDs can be modeled by a shunt impedance, $Z_{res}$, connected to the transmission line (Grabovskij et al. (2008)). The transfer function is written as a function of an injected frequency,

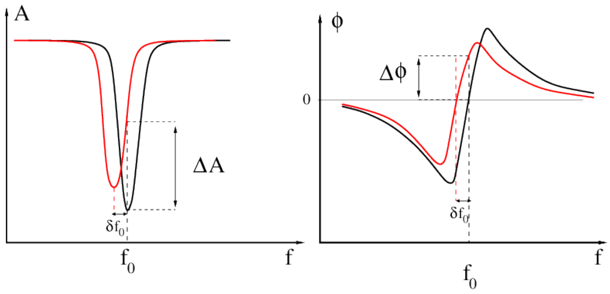


**Fig. 1.** Amplitude and phase of the transfer function of KIDs under dark conditions (black) and under illumination (red).

$f$, the resonance frequency, $f_0$, and a set of parameters, $\boldsymbol{p} = (X_1, X_2, Z_0, Q_i, Q_e)$

$$S_{21}(f; f_0, \boldsymbol{p}) = \frac{2Z_{\rm res}Z_0}{Z_{\rm res}(2Z_0 + j(X_1 + X_2)) + (Z_0 + jX_1)(Z_0 + jX_2)} \quad (2)$$

with the shunt impedance written as

$$Z_{\rm res} = \frac{Z_0 Q_{\rm e}}{2Q_{\rm i}}\left(1 + 2jQ_{\rm i}\frac{f_0 - f}{f_0}\right) \quad (3)$$

The parameters $X_1$, $X_2$ and $Z_0$ are impedances accounting for the connections; $Q_{\rm i}$ is the intrinsic quality factor of the resonator and $Q_{\rm e}$ is the external quality factor due to the coupling with the readout electronics (the description of the electronics can be found in (Bourrion et al. (2011))). The real and imaginary parts of the transfer function are respectively noted $I = \mathcal{R}e(S_{21}) + I_c$ (In-phase) and $Q = \mathcal{I}m(S_{21}) + Q_c$ (Quadrature), where $I_c$ and $Q_c$ account for a given offset. The amplitude is then given by $A = \sqrt{I^2 + Q^2}$ and the phase by $\phi = \mathrm{atan}\left(\frac{Q}{I}\right)$.

Figure 1 represents the amplitude and the phase of the KID transfer function under two different conditions. The black line correspond to the resonance under dark conditions and the red one when the detector is illuminated. In the case of exciting the detector with a frequency equal to the resonance frequency $f_0$, illumination leads to a change in the measured amplitude $\Delta A$ and phase $\Delta\phi$ of the transfer function.

Figure 2 represents an example of $I$ and $Q$ as a function of the exciting frequency $f$. These data have been taken during a frequency scan, they are given for a frequency range which contains a resonance in the transmission line, corresponding to a single KID. The parameters of the model given by equation 2 can be obtained for individual KIDs by fitting the resonances. The green line, in figure 2, gives the result of the least square fit of $I$ and $Q$. In this case $Z_0$ is fixed to 50 Ω and we impose $X_1 = X_2$, we obtained $X_1 = X_2 = 3.0$ Ω, $Q_{\rm e} = 5.2 \times 10^4$, $Q_{\rm i} = 1.0 \times 10^5$ and $f_0 = 1.2729985$ GHz. For the array used here, the values of the parameters do not change significantly for different KIDs. The typical values of the parameters obtained in this example are $Z_0 = 50$ Ω (fixed), $X_1 = X_2 \sim 3$ Ω, $Q_{\rm e} \sim 5 \times 10^4$, $Q_{\rm i} \sim 1 \times 10^5$ and $f_0 \sim 1.27$ GHz.

### *2.2. Simulation of the transmission line*

The transfer function of the full line (KIDs and transmission) can be modeled as

$$S_l(f) = A_l(f)e^{i\theta_l(f)} \times \prod_{k=1}^{N_k} S_{12,k}(f; \boldsymbol{p}_k) \quad (4)$$

where $k$ labels the KIDs and $N_k$ is the number of detector. The parameters $A_l(f)$ and $\theta_l(f)$ give the amplitude and the phase of

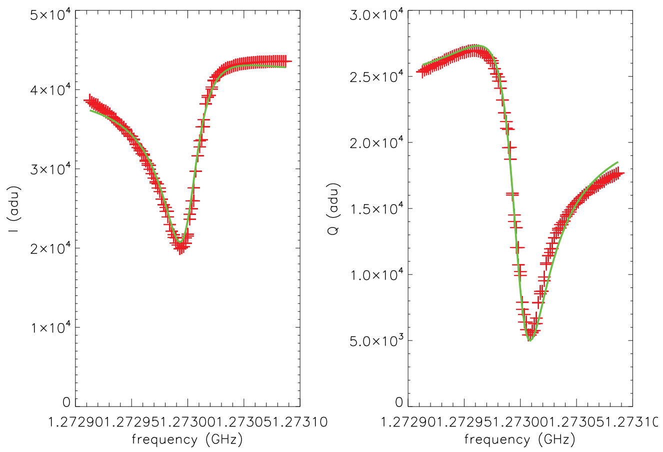


**Fig. 2.** Frequency scan of the real part ($I$) and the imaginary part ($Q$) of the transfer function of a resonance of the transmission line, corresponding to a KID. The data points are represented in red for $I$ and $Q$ as a function of the excitation frequency $f$. The green line gives the simultaneous least square fit of $I$ and $Q$ as a function of excitation frequency, with the model given by equation 2. Here $Z_0$ is fixed to 50 Ω and we impose $X_1 = X_2$, the parameters obtained in this example are $X_1 = X_2 = 3.0$ Ω, $Q_{\rm e} = 5.2 \times 10^4$, $Q_{\rm i} = 1.0 \times 10^5$ and $f_0 = 1.2729985$ GHz.

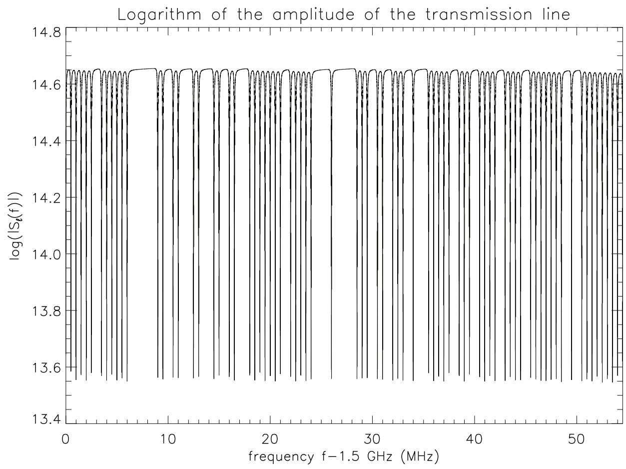


**Fig. 3.** Example of a simulated transmission line. Each KID is similar with parameters $Z_0 = 50$ Ω, $X_1 = X_2 = 3$ Ω, $Q_{\rm e} = 5 \times 10^4$ and $Q_{\rm i} = 1 \times 10^5$. The resonance frequencies are separated by 0.5 MHz starting from 1.5 GHz. We can see holes in the line which correspond to off resonance or blind KIDs.

the transmission line and each detector is modeled by equation 2 with specific parameters. Figure 3 gives an example of a simulated transmission line where all the KIDs are identical with their resonance frequency regularly distributed along the line, except for holes in the line which correspond to blind or off resonance detectors.

## 3. Simulation of the TOIs with NIKA

### *3.1. Simulation of the instrument*

The simulation is based on the data taken during the run of October 2011. NIKA is simulated by:

- 2 arrays at 140 GHz and 220 GHz. The bandwidths are supposed to be infinitely narrow for both observation frequencies.
- The number and the location of the detectors in the focal plane are taken from real data: the size of the camera in the focal plane is about 2 arcmin an the detectors are separated by about 13 arcsec. The only KIDs considered here are the KIDs which are working normally and the off resonance KIDs.
- The scan strategy is similar to the one used in practice at the IRAM 30-m telescope.

The following method is adopted: we first construct temperature Rayleigh-Jeans TOIs according to the scan strategy used here (*i.e.* the optical signal). Then the TOIs are converted into shift of the resonance frequency TOI for each detector, taking into account the different responses of the KIDs. From equation 4, the TOIs $I(t)$ and $Q(t)$ are obtained for injected frequencies $f_k$ corresponding to the detector resonances. Finally, the shift of the resonance frequency TOIs of each KID are reconstructed using $I(t)$ and $Q(t)$; this will be further developed in Section 4.

### 3.2. Modeling the sources of noise

#### 3.2.1. Atmospheric noise

The atmospheric noise is due to the thermal emission of clouds of water vapor which pass by the telescope field of view. The speed of these clouds is much larger than the speed of the scan of the telescope such that the corresponding noise almost only depends on time. However, since all detectors do not have the exact same position in the focal plane, the atmospheric noise is different for each KID. At first order, this effect depends linearly on the distance between the considered KIDs and the center of the array. We simulate the atmospheric noise using a noise map passing by the telescope with a given velocity. The spatial power spectrum of the atmospheric contribution is given by

$$\begin{cases} \tilde{A} \propto k^{\alpha} \\ \alpha \simeq -0.8 \end{cases} \tag{5}$$

The atmospheric noise is added for each detector to the Kelvin Rayleigh Jeans ($K_{RJ}$) TOIs since it is an optical contribution. Its amplitude is adjusted typically to a few $K_{RJ}$ at 140 GHz for a 15 minutes scan and we suppose it is proportional to $\nu^2$.

#### 3.2.2. Instrumental noise

The instrumental noise arises from the KIDs themselves and from the electronics. It can be divided into a non correlated white noise, $N_{dec}$, different for all detectors, and a correlated noise, $N_{cor}$, which is proportional for all KIDs and follow a $1/f$ power spectrum. In this case, the noise is added to the $I(t)$ and $Q(t)$ TOIs because it arises from the instrument. Once again, the given values have been estimated from the run of October 2011. We have for both $I(t)$ and $Q(t)$

$$\begin{cases} \tilde{N}_{i=\mathrm{cor,dec}} \propto f^{\beta_i} & \\ \beta_{\mathrm{cor}} \simeq -0.1 & \tilde{N}_{\mathrm{cor}}(1\ \mathrm{Hz}) \simeq 400\ [\mathrm{adu}].\mathrm{Hz}^{-1/2} \\ \beta_{\mathrm{dec}} = 0 & \tilde{N}_{\mathrm{dec}} \simeq 110\ [\mathrm{adu}].\mathrm{Hz}^{-1/2} \end{cases} \tag{6}$$

Note that $I(t)$ and $Q(t)$ are dimensionless[2], we will see in Section 4 how they are used to reconstruct the shift of the resonance frequency TOIs and therefore the temperature Rayleigh-Jeans TOIs.

### 3.3. Final TOIs

The Rayleigh-Jeans temperature TOIs are then converted into shift of the resonance frequency TOI via the pointing matrix $P_k(x_k, y_k, t)$, the coefficient $\Gamma_\nu$ taken from a reference detector for each array ($\Gamma_{140\mathrm{GHz}} = 670\ \mathrm{Hz.K}_{Rj}^{-1}$ and $\Gamma_{220\mathrm{GHz}} = 500\ \mathrm{Hz.K}_{Rj}^{-1}$) and the coefficients $\lambda_k$ which are known experimentally and account for the fact that all KIDs do not have the same response to optical power. We can write the shift of the resonance frequency TOIs as

$$\delta f_{0k}(t) = \Gamma_\nu \lambda_k P_k(x_k, y_k, t)\left[S_{\mathrm{astro}}(x_k, y_k) + S_{\mathrm{atmo}}(x_k, y_k, t)\right] \tag{7}$$

where $k$ labels the KIDs (*i.e.* the injected exciting frequency or the tone). The quantity $S_{\mathrm{astro}}(x_k, y_k)$ is the signal due to the target astrophysical source and $S_{\mathrm{atmo}}(x_k, y_k, t)$ the atmospheric noise.

The TOIs $I_{optic}(t)$ and $Q_{optic}(t)$ are then computed from equation 4 as the real and imaginary part of the transfer function. The resonance frequency is the sum of an initial frequency, set to the injected frequency $f_k$ (corresponding to the resonance frequency of each detector), and the shift of the resonance frequency given by equation 7. The final $I(t)$ and $Q(t)$ TOIs are then given by

$$\begin{cases} I_k(t) = I_{optic}(t) + \mu_k N_{I,cor}(t) + \chi_k N_{I,dec}(t) \\ Q_k(t) = Q_{optic}(t) + \mu_k N_{Q,cor}(t) + \chi_k N_{Q,dec}(t) \end{cases} \tag{8}$$

where $\mu_k$ and $\chi_k$ give the relative amplitudes of the electronic and intrinsic detector noise respectively.

## 4. Measurement of the absorbed optical power

### 4.1. Reconstruction of the shift of the resonance frequency

In practice, the full resonance cannot be monitored permanently during observations. In order to estimate the shift of the resonance frequency $\delta f_0$, the following strategy is used Calvo et al. (2012). The transfer function of each KID is sampled at 880 Hz, this gives the real and imaginary parts of $S_I(f_k)$ noted $i_k(t)$ and $q_k(t)$ (*c.f.* equation 8). The excitation frequency generated by a local oscillator $f_{\mathrm{LO}}^k$ falls into the resonance of each KID $k$ and is modulated such that it takes alternatively the values $f_-^k = f_{LO}^k - \delta f_{\mathrm{LO}}/2$ and $f_+^k = f_{\mathrm{LO}}^k + \delta f_{LO}/2$. The quantity $\delta f_{\mathrm{LO}} = 2$ kHz in our case and in the simulation, $f_{\mathrm{LO}}^k$ is set to the exact resonance frequency of the KID $k$ under dark conditions; this is not exactly the case in practice. The 880 Hz samples are then used to compute the averaged $I$ and $Q$ over $N_{\mathrm{m}} = 40$ points, and the averaged difference between samples at $f_-$ and samples at $f_+$.

$$\begin{cases} I = \sum_{p=1}^{N_{\mathrm{m}}} i_p \\ Q = \sum_{p=1}^{N_{\mathrm{m}}} q_p \\ \delta I = \sum_{p=1}^{N_{\mathrm{m}}/2} i_{2p} - i_{2p-1} \\ \delta Q = \sum_{p=1}^{N_{\mathrm{m}}/2} q_{2p} - q_{2p-1} \end{cases} \tag{9}$$

Figure 4 represents the resonance in the $I - Q$ plane. Red points are averaged $I$ and $Q$ (22 Hz) measured with a fixed difference of the shift of the resonance frequency $\Delta(\delta f_0)$, however the distance between these points is not constant. We define the vectors

[2] In practice $I(t)$ and $Q(t)$ are measured in volts, the amplitudes of the noises are given according to these units used in practice.

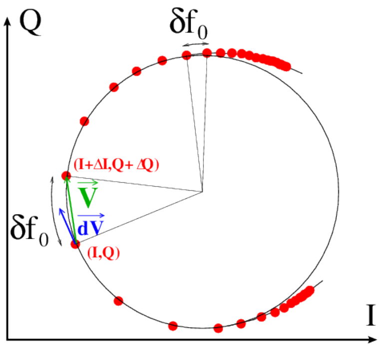


**Fig. 4.** $I-Q$ plane around the resonance. Red points give $I$ and $Q$ sampled at 22 Hz for which the difference of the shift of the resonance frequency $\Delta(\delta f_0)$ is constant between two consecutive points. Vectors $\boldsymbol{V} = (\Delta I, \Delta Q)$ and $\boldsymbol{\delta V} = (<\delta I>, <\delta Q>)$ are represented.

$\boldsymbol{V} = (\Delta I, \Delta Q)$ and $\boldsymbol{\delta V} = (<\delta I>, <\delta Q>)$ where $\Delta I$ and $\Delta Q$ stands for the difference between two consecutive points at 22 Hz[3]. In the case of small differences between consecutive points, $\delta f_0$ is proportional to the projection of $\boldsymbol{V}$ on the axis directed by $\boldsymbol{\delta V}$, given by $\frac{\boldsymbol{\delta V}.\boldsymbol{V}}{|\boldsymbol{\delta V}|}$. Normalizing this quantity by $\left|\left(\frac{dI}{df}, \frac{dQ}{df}\right)\right| \equiv \frac{|\boldsymbol{\delta V}|}{\delta f_{\mathrm{LO}}}$ allows us to measure difference of the shift of the resonance frequency between two point sampled at 22 Hz. Finally we can write

$$\Delta\left(\delta f_0^{\mathrm{meas}}\right) = \delta f_{\mathrm{LO}} \frac{\boldsymbol{\delta V}.\boldsymbol{V}}{|\boldsymbol{\delta V}|^2} = \delta f_{\mathrm{LO}} \frac{\Delta I <\delta I> + \Delta Q <\delta Q>}{<\delta I>^2 + <\delta Q>^2} \tag{10}$$

The shift of the resonance frequency as a function of time is then computed by integrating the differences between the 22 Hz sampled data, given by

$$\delta f_0^{\mathrm{meas}}(t) = \sum_{t^\star=0}^{t} \Delta\left(\delta f_0^{\mathrm{meas}}\right)(t^\star) \tag{11}$$

Figure 5 gives, on the left hand side, the $\delta f_0^{\mathrm{meas}}{}_k(t)$ TOIs in the case of the observation of the cluster Abell 665 during the run of October 2011. The right hand side shows the $\delta f_0^{\mathrm{meas}}{}_k(t)$ TOIs in the case of the simulation of the observation of a cluster. In both cases, the given TOIs are represented for four KIDs of the 140 GHz array, with different amplitude due to the response (described by $\lambda_k$ in the simulation). The astrophysical signal is drawn within the atmospheric and instrumental noises. The real data contain glitches while they have not been taken into account in the simulation. However they are easily removed in practice.

Figure 6 represents the power spectrum associated to the TOIs given in Figure 5. We can see the contribution of the different sources of noise, given by the different slopes, in both real and simulated data. Note that the real data power spectrum contains lines at $\sim$ 1.5 Hz and its harmonics, due to mechanics of the cryostat, which are not included in the simulation.

According to figure 5 and figure 6, the simulation is consistent with real data, within the approximations made here.

### *4.2. Validity range of the measurement method*

It is important to emphasize that the method described above can break down in certain situations. First, it assumes that the sources observed are faint, otherwise the misalignment of the vectors $\boldsymbol{\delta V}$ and $\boldsymbol{V}$ becomes too large (*i.e.* the optical load shifts the resonances such that it becomes larger than the width of the resonance, see Figure 1). Then, the time line is built via Equation 11, integrating small differences. Brutal changes during the observations might lead to bias in the method. Finally, the losses in the superconductors increases under illumination. This leads to a change of the radius of the $I-Q$ circle given in Figure 4. However, this effect does not account for more than 2% bias; it has not been simulated in the work presented here (*i.e.* all parameters $\boldsymbol{p}$ in equation 2 are held constant for a given KID).

In order to test the validity of the method, we propose to simulate the observations of point sources with different temperatures, without noise, monitored by the maximum value taken by $\delta f_0(t)$ (in order to check the faint source assumption) and for different speed of the scan $v_s$ (in order to check the impact of brutal changes during observations). Let $\delta f_0^{\mathrm{meas}}(t)$ be the measured shift of the resonance frequency described in Section 4.1, during the scan of the source, and $\delta f_0^{\mathrm{exp}}(t)$ the expected shift. We define the quantities

$$\begin{cases} \xi_{\mathrm{int}} = \dfrac{\int \delta f_0^{\mathrm{meas}}(t)dt}{\int \delta f_0^{\mathrm{exp}}(t)dt} \\ \xi_{\mathrm{amp}} = \dfrac{\max\left(\delta f_0^{\mathrm{meas}}(t)\right)}{\max\left(\delta f_0^{\mathrm{exp}}(t)\right)} \end{cases} \tag{12}$$

which we will use as validity criteria. In the case of accurate photometry, we expect $\xi_{\mathrm{int}}$ and $\xi_{\mathrm{amp}}$ to be close to 1. The panels left and right of Figure 7 represents respectively the value of $\xi_{\mathrm{int}}$ and $\xi_{\mathrm{amp}}$ in the plan $\left(\log\left(\frac{v_s}{1\ \mathrm{arcsec.s^{-1}}}\right), \log\left(\frac{\max\left(\delta f_0^{\mathrm{exp}}(t)\right)}{1\ \mathrm{Hz}}\right)\right)$. The typical speed of scan at the IRAM 30-meters telescope is $\sim$ 10 arcsec.s$^{-1}$, so the flux measured is in agreement with the expected flux at 1% for most cases of interest. Even for planets which are the strongest sources, $\max\left(\delta f_0^{\mathrm{exp}}(t)\right) \sim 5 \times 10^3$ Hz, the photometry is accurate within a few percents error.

Since we are interested in the observation of sources much fainter than planets, the method described in Section 4.1 appears to be accurate within a few percent.

## 5. Conclusions

We have constructed the simulation of the observation pipeline of the NIKA camera. The detectors have been modeled with a transfer function and coupled to a single transmission line. The different sources of noise have been taken into account and adjusted according to the run of October 2011. The method used to recover the absorbed optical power has been tested using a simulation of KIDs. It is consistent with observations of real sources and appears to be valid in non extremal cases such as the observation of galaxy clusters.

## References

Bourrion, O., Bideaud, A., Benoit, A., et al. 2011, JINST, 6, P06012
Calvo, M., Giordano, C., Battiston, R., et al. 2010, Experimental Astronomy, 28, 185
Calvo, M., Roesch, M., Désert, F. X., et al. 2012, A&A
Doyle, S., Mauskopf, P., & Naylon, J. 2008, J. Low Temp. Phys., 151, 530
Grabovskij, G. J., Swenson, L. J., Buisson, O., et al. 2008, Appl. Phys. Lett., 93, 134102
Monfardini, A., Benoit, A., Bideaud, A., et al. 2011, ApJS, 194, 24
Monfardini, A., Swenson, L. J., Bideaud, A., et al. 2010, A&A, 521, A29
Staguhn, J. G., Benford, D. J., Allen, C. A., et al. 2006, in Society of Photo-Optical Instrumentation Engineers (SPIE) Conference Series, Vol. 6275, Society of Photo-Optical Instrumentation Engineers (SPIE) Conference Series
Swenson, L. J., Cruciani, A., Benoit, A., et al. 2010, Appl. Phys. Lett., 96, 263511

[3] $<.>$ means that the values are smoothed using 50 points before and after the considered point.

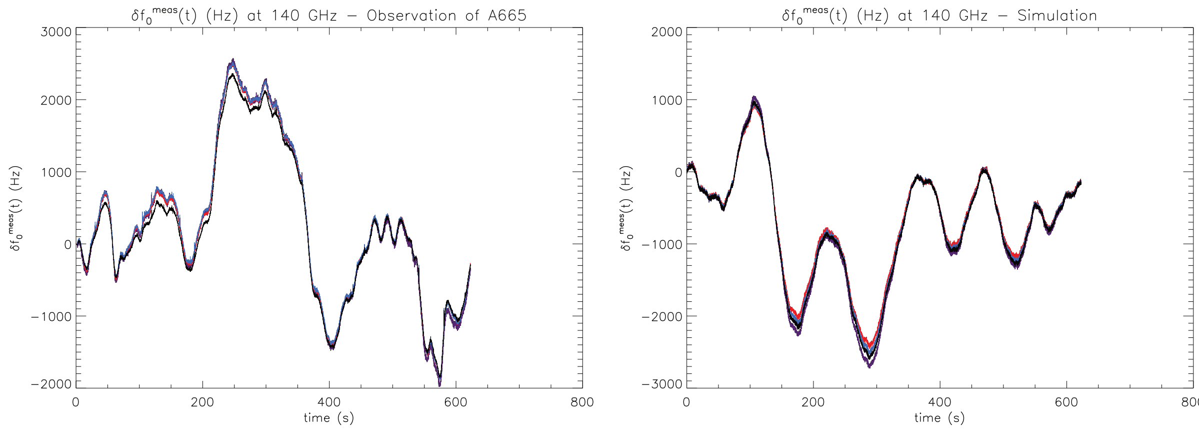


**Fig. 5.** Left panel: $\delta f_{0\ k}^{\rm meas}(t)$ TOIs in the case of real data taken during the run of October 2011 for the observation of the galaxy cluster Abell 665. Right panel: $\delta f_{0\ k}^{\rm meas}(t)$ TOIs in the case of the simulation of the observations of a cluster of galaxies. In both cases the TOIs correspond to the four KIDs at the extremities of the 140 GHz array.

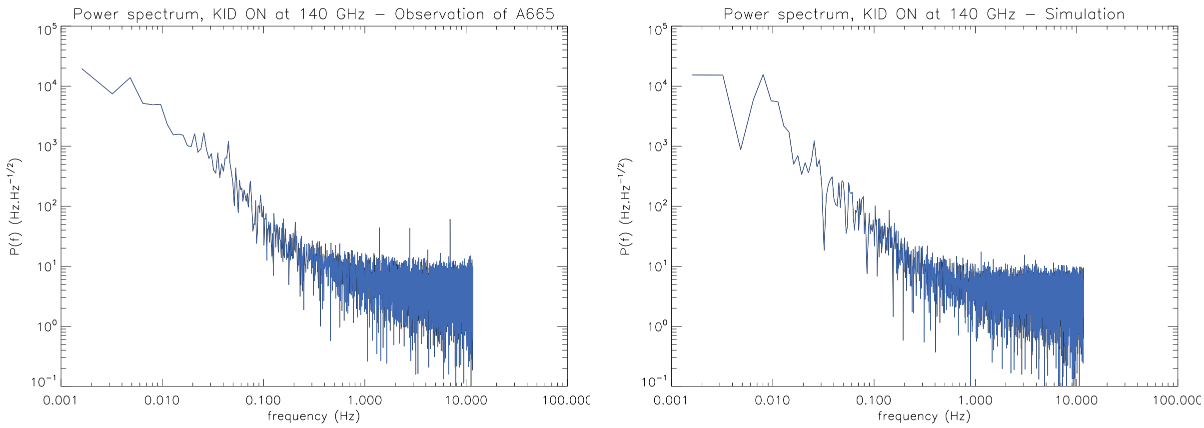


**Fig. 6.** Left panel: power spectrum associated to $\delta f_0^{\rm meas}(t)$ TOIs in the case of real data taken during the run of October 2011 for the observation of the galaxy cluster Abell 665 (Figure 5, left). Right panel: power spectrum associated to $\delta f_0^{\rm meas}(t)$ TOIs in the case of the simulation of the observation of a cluster of galaxies (Figure 5, right). We can see in both cases the different slopes corresponding to the different sources of noise.

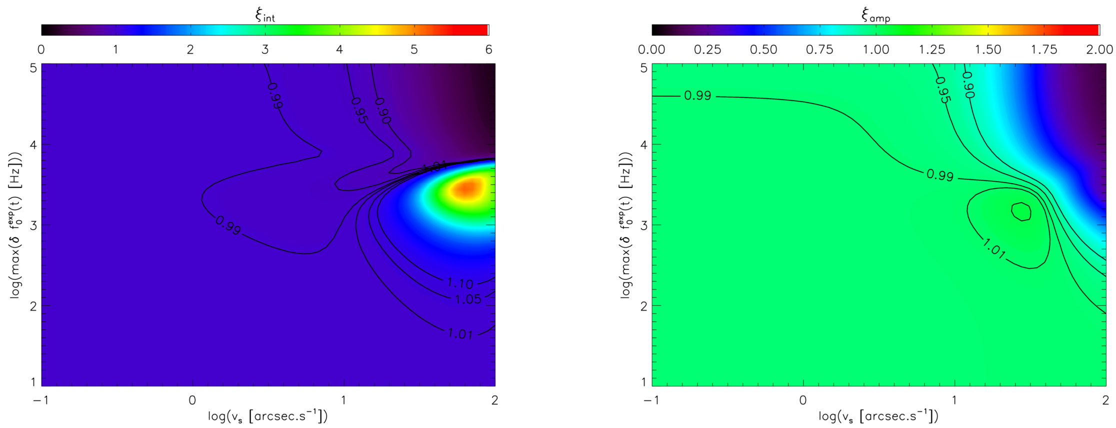


**Fig. 7.** Left panel: $\xi_{\rm int} = \frac{\int \delta f_0^{\rm meas}(t)dt}{\int \delta f_0^{\rm exp}(t)dt}$ given in the plane $\left(\log\left(\frac{v_s}{1\ {\rm arcsec.s^{-1}}}\right), \log\left(\frac{\max\left(\delta f_0^{\rm exp}(t)\right)}{1\ {\rm Hz}}\right)\right)$. Right panel: $\xi_{\rm amp} = \frac{\max\left(\delta f_0^{\rm meas}(t)\right)}{\max\left(\delta f_0^{\rm exp}(t)\right)}$ given in the same plane. Iso-contours at 0.9, 0.95, 0.99, 1.01, 1.05 and 1.1 are represented. The KID used here is modeled by the transfer function of Equation 2 with the parameters $Z_0 = 50\ \Omega$, $Q_{\rm i} = 2 \times 10^5$, $Q_{\rm e} = 5 \times 10^4$, $f_0 = 1.5 \times 10^9$, and $X_1 = X_2 = 3\ \Omega$.